

# Supplementary Materials: Utilizing Earth Observations of Soil Freeze/Thaw data and Atmospheric Concentrations to Estimate Cold Season Methane Emissions in the Northern High Latitudes

Maria Tenkanen<sup>1,\*</sup>, Aki Tsuruta<sup>1</sup>, Kimmo Rautiainen<sup>2</sup>, Vilma Kangasaho<sup>1</sup>, Raymond Ellul<sup>3</sup> and Tuula Aalto<sup>1</sup>

**Table S1.** List of surface observation sites used in inversions, located below 49°N. Observation Uncertainty (Obs. Unc.) is used to define diagonal values in the observation covariance matrix. Data type is categorized into two measurements (discrete (D) and continuous (C)).

Sitecode	Site Name	Country	Contributor	Longitude [°E]	Latitude [°N]	Height* [m a.s.l.]	Obs. Unc. [ppb]	Data type D/C	Date min.** [yyyy/mm]	Date max. [yyyy/mm]
AMS	Amsterdam Island	France	LSCE	77.54	-37.80	75	4.5	C	2012/01	2018/04
AMS	Amsterdam Island	France	LSCE	77.54	-37.80	700, 75.0	4.5	D	2001/03	2016/04
AMT	Argyle, Maine	United States	NOAA/GML	-68.68	45.03	160.0, 156.97	157.0	P	2008/11	2018/12
AMY	Anmyeon-do	Republic of Korea	NOAA/GML	126.33	36.54	87	30.0	D	2013/12	2018/12
ARH	Arrival Heights	New Zealand	NIWA	166.66	-77.83	189	4.5	D	1999/01	2019/12
ASC	Ascension Island	United Kingdom	NOAA/GML	-14.40	-7.97	90	15.0	D	1998/01	2018/12
ASK	Assekrem	Algeria	NOAA/GML	5.63	23.26	2715	25.0	D	1998/01	2018/12
AZR	Terceira Island, Azores	Portugal	NOAA/GML	-27.38	38.77	24	15.0	D	1998/01	2018/12
BCU	Begur	Spain	LSCE	3.23	41.97	150, 13.0	15.0	D	2000/04	2016/07
BDUD	Bergen Head Station	New Zealand	NOAA/GML	174.87	41.41	90.0, 95.0	4.5	D	2003/03	2018/12
BKT	Bukit Kotahsing	Indonesia	NOAA/GML	100.32	-0.20	825	75.0	D	2004/01	2018/12
BKT	Bukit Koto Tabang	Indonesia	BMKG-Empa	100.32	-0.20	896	75.0	C	2009/10	2019/12
BMW	Tudor Hill, Bermuda	United Kingdom	NOAA/GML	-64.88	32.26	33.0, 51.34	60.0	D	1998/01	2018/12
BSC	Black Sea, Constanta	Romania	NOAA/GML	28.66	44.18	5	75.0	D	1998/01	2011/12
CFA	Cape Ferguson, Queensland	Australia	CSIRO	147.06	-19.28	5	25.0	D	1998/02	2018/12
CGO	Cape Grim, Tasmania	Australia	NOAA/GML	144.69	-40.68	164	4.5	D	1998/01	2018/12
CGR	Cape Granitola	Italy	Institute for Atmospheric Sciences and Climate (ISAC)	12.65	37.67	9	25.0	C	2015/04	2018/12
CIR	Clipperton Island	Republic of Kiribati	NOAA/GML	-157.15	1.70	5	15.0	D	1998/11	2018/12
CMN	Mt. Cimone Station	Italy	University of Urbino	10.70	44.19	2172	15.0	C	2003/07	2017/12
CMN	Mt. Cimone Station	Italy	ICOS-ATC, CNR-ISAC	10.70	44.19	2173	15.0	C	2018/05	2018/12
COI	Cape Ochiishi	Japan	NIES	145.50	43.16	94	15.0	C	1998/12	2018/01
CPT	Cape Point	South Africa	NOAA/GML	18.49	-34.35	260	25.0	D	2010/02	2018/12
CPT	Cape Point	South Africa	SAWS	18.49	-34.35	260	15.0	C	1999/01	2019/12
CRI	Cape Rama	India	CSIRO	73.83	15.08	66	75.0	D	1998/01	2013/01
CRZ	Crozet Islands	France	NOAA/GML	51.85	-46.43	202	4.5	D	1998/01	2018/12
CYA	Cape, Antarctica	Australia	CSIRO	110.52	-66.28	55	4.5	D	1998/01	2018/11
DOW	Downsville	Canada	ECCC	-79.47	43.74	218	25.0	C	2003/10	2018/03
EGB	Eggen, Ontario	Canada	ECCC	-79.76	44.23	276.0, 254.0	25.0	D	2005/03	2018/12
EIC	Easter Island	Chile	NOAA/GML	-109.43	-27.16	72.0, 69.0	4.5	D	1998/01	2018/12
FKL	Finsaskala	Greece	LSCE, ECP1/UOC	25.67	35.34	165	15.0	C	2014/06	2018/04
GLH	Giordan Lighthouse	Malta	University of Malta	14.22	36.07	167	15.0	C	2012/10	2017/12
GMI	Mariana Islands	Guam	NOAA/GML	144.66	13.39	8.0, 6.0, 5.0	15.0	D	1998/01	2018/12
GPA	Gunn Point	Australia	CSIRO	131.05	-12.25	37	75.0	D	2010/08	2016/06
HAT	Hateruma	Japan	NIES	123.81	24.06	47.3	15.0	C	1998/12	2018/01
HBA	Halley Station, Antarctica	United Kingdom	NOAA/GML	-26.21	-75.61	35	4.5	D	1998/01	2018/12
HNP	Hanlan's Point, Ontario	Canada	ECCC	-79.39	43.61	97	25.0	C	2014/06	2018/12
HPB	Hohenpeissenberg	Germany	NOAA/GML	11.02	47.80	941	25.0	D	2006/04	2018/12
HPB	Hohenpeissenberg	Germany	ICOS-ATC, HPB	11.02	47.80	1065	25.0	C	2015/09	2018/12
HNH	Heg-hatal	Hungary	NOAA/GML	16.65	46.95	344	75.0	D	1998/01	2018/12
HUN	Iopra	Italy	ICOS-ATC, JRC	8.63	45.81	310	30.0	C	2017/12	2018/12
IZO	Izana, Tenerife, Canary Islands	Spain	NOAA/GML	-16.50	28.31	2377.9	15.0	D	1998/01	2018/12
IZO	Izana, Tenerife, Canary Islands	Spain	AEMET	-16.50	28.31	2386.0, 2403.0, 2381.0	25.0	C	1999/01	2019/12
IJF	Jungfraujoch	Switzerland	EMPA	7.99	46.55	3586	15.0	C	2014/01	2017/12
IJF	Jungfraujoch	Switzerland	ICOS-ATC, HFSJG	7.99	46.55	3585	15.0	C	2016/12	2018/12
KYE	Key Biscayne, Florida	United States	NOAA/GML	-80.16	25.67	6	25.0	D	1998/01	2018/12
KUM	Cape Kumukahi, Hawaii	United States	NOAA/GML	-155.01	19.74	8.0, 5.3, 3.0, 41.1	15.0	D	1998/01	2018/12
LAU	Lauder	New Zealand	NIWA	169.68	-45.04	380	15.0	D	2009/05	2019/12
LFB	Park Falls, Wisconsin	United States	UW-MT	-90.27	45.95	868	30.0	D	2006/06	2018/12
LBN	Lulu, Taiwan	Taiwan	NOAA/GML	120.87	23.47	2867	25.0	D	2006/08	2018/12
LMP	Lampedusa	Italy	NOAA/GML	12.62	35.52	50	25.0	D	2006/10	2018/12
LMT	Laemza Terme	Italy	ISAC	16.23	38.88	14	30.0	C	2015/01	2016/12
LPO	Ile Grande	France	LSCE	-3.58	48.80	20	15.0	D	2004/11	2013/08
MAA	Mawson Station, Antarctica	Australia	CSIRO Oceans and Atmosphere	62.87	-67.62	42	4.5	D	1998/01	2018/12
MEX	High Altitude Global Climate Observation Center	Mexico	NOAA/GML	-97.31	18.98	4469	15.0	D	2009/01	2018/12
MID	Sand Island, Midway	United States	NOAA/GML	-177.38	28.21	8.0, 15.3, 16.0	15.0	D	1998/01	2018/12
MKN	Mt. Kenya	Kenya	NOAA/GML	37.30	-0.06	3649	25.0	D	2003/12	2011/06
MLO	Mauna Loa, Hawaii	United States	NOAA/GML	-155.58	19.54	3437	15.0	C	1998/01	2018/12
MLO	Mauna Loa, Hawaii	United States	NOAA/GML	-155.58	19.54	3402.0, 3437.0	15.0	D	1998/01	2018/12
MNN	Minamitorishima	Japan	Environment Division Global Environment and Marine Department Japan Meteorological Agency (JMA)	153.98	24.28	27.1	15.0	C	1998/01	2018/12
MQA	Macquarie Island	Australia	CSIRO	158.97	54.48	13	4.5	D	1998/01	2018/12
NAT	Farol De Mae Laizza Lighthouse	Brazil	NOAA/GML	-35.19	-5.80	20, 87.0	15.0	D	2010/09	2018/12
NMB	Gobabeb	Namibia	NOAA/GML	15.03	-23.58	461	25.0	D	1998/07	2018/12
NWR	Niwot Ridge, Colorado	United States	NOAA/GML	-105.59	40.05	3526	15.0	D	1998/01	2018/12
OPE	Observatoire perenne de l'environnement	France	ICOS-ATC, LSCE	5.50	48.56	510	30.0	C	2016/08	2018/12
PDI	Pha Din	Viet Nam	VNMHA	103.52	21.57	1478	75.0	C	2014/02	2019/12
PDM	Pic du Midi	France	LSCE	0.14	42.94	2887.0, 2877.0	15.0	D	2001/06	2014/12
PRS	Plateau Rose	Italy	Ricerca sul Sistema Energetico (RSE)	7.71	45.94	3490	15.0	C	2005/01	2018/12
PSA	Palmer Station, Antarctica	United States	NOAA/GML	-64.00	-64.92	15	4.5	D	1998/01	2018/12
PTA	Point Arena, California	United States	NOAA/GML	-123.74	38.95	22	25.0	D	1999/01	2011/05
PUY	Puy de Dome	France	ICOS-ATC, LSCE	2.97	45.77	1475	15.0	C	2016/08	2018/12
RPB	Ragged Point	Barbados	NOAA/GML	-59.43	13.17	20	15.0	D	1998/01	2018/12
RYO	Ryori	Japan	JMA	141.82	39.03	280	15.0	C	1998/01	2018/12
SDZ	Shangdianzi	Peoples Republic of China	NOAA/GML	117.12	40.65	298	15.0	D	2009/09	2015/09
SEY	Mahe Island	Seychelles	NOAA/GML	55.53	-4.68	7	15.0	D	1998/01	2018/12
SGP	Southern Great Plains, Oklahoma	United States	NOAA/GML	-97.49	36.61	374.0, 339.0	75.0	D	2002/04	2018/12
SMD	Tutuila	American Samoa	NOAA/GML	-170.56	-14.25	47.0, 60.3	15.0	D	1998/01	2018/12
SNB	Sonneblick	Austria	University of Innsbruck Austria/Environment	47.05	12.96	3111	15.0	C	2012/04	2019/12
SPO	South Pole, Antarctica	United States	NOAA/GML	-24.80	-89.90	2821.3, 2815.0	4.5	D	1998/01	2018/12
SSL	Schauinsland	Germany	UBA-Germany	7.92	47.90	1217.0, 1211.0, 1215.5	30.0	C	1999/01	2018/12
SYO	Syowa Station, Antarctica	Japan	NOAA/GML	39.59	69.01	16.0, 19.0	4.5	D	1998/01	2018/12
TAP	Tae-ahn Peninsula	Republic of Korea	NOAA/GML	126.13	36.74	21	75.0	D	1998/01	2018/12
THD	Trinidad Head, California	United States	NOAA/GML	-124.15	41.05	112	25.0	D	2002/04	2017/06
TLL	El Tololo	Chile	Dirección Meteorológica de Chile (DMC)	-70.80	-30.17	2159	25.0	C	2013/04	2019/09
TRN	Trainou	France	ICOS-ATC, LSCE	2.11	47.96	311	25.0	C	2016/08	2018/12
TPP	Turkey Point	Canada	ECCC	-80.33	42.68	266	15.0	C	2012/11	2018/05
USH	Ushuaia	Argentina	NOAA/GML	-68.31	-54.35	32	4.5	D	1998/01	2018/12
UTA	Wendover, Utah	United States	NOAA/GML	-113.72	39.90	1332	25.0	D	1998/01	2018/12
UUM	Ulaan Uul	Mongolia	NOAA/GML	111.10	44.45	1012	25.0	D	1998/01	2018/12
WIS	Weizmann Institute of Science at the Arava Ins...	Israel	NOAA/GML	35.06	29.96	482.0, 156.0	25.0	D	1998/01	2018/12
WKT	Moody, Texas	United States	NOAA/GML	-97.33	31.31	708.1	75.0	P	2007/09	2018/03
WLG	Mt. Waliguan	Peoples Republic of China	NOAA/GML	100.90	36.29	3890.0, 3815.0	15.0	D	1998/01	2018/12
WSA	Sable Island, Nova Scotia	Canada	ECCC	-60.01	43.93	8.0, 30.0	25.0	C	2003/06	2018/12
YON	Yonagunijima	Japan	JMA	123.02	24.47	50	30.0	C	1998/01	2018/12
ZSF	Zugspitze / Schneefernerhaus	Germany	UBA-Germany	10.98	47.42	2670	30.0	C	2002/01	2019/12

\*Sampling heights from which atmospheric CH<sub>4</sub> is sampled in TM5. \*\*Observations used in this study between 2010 and 2018.

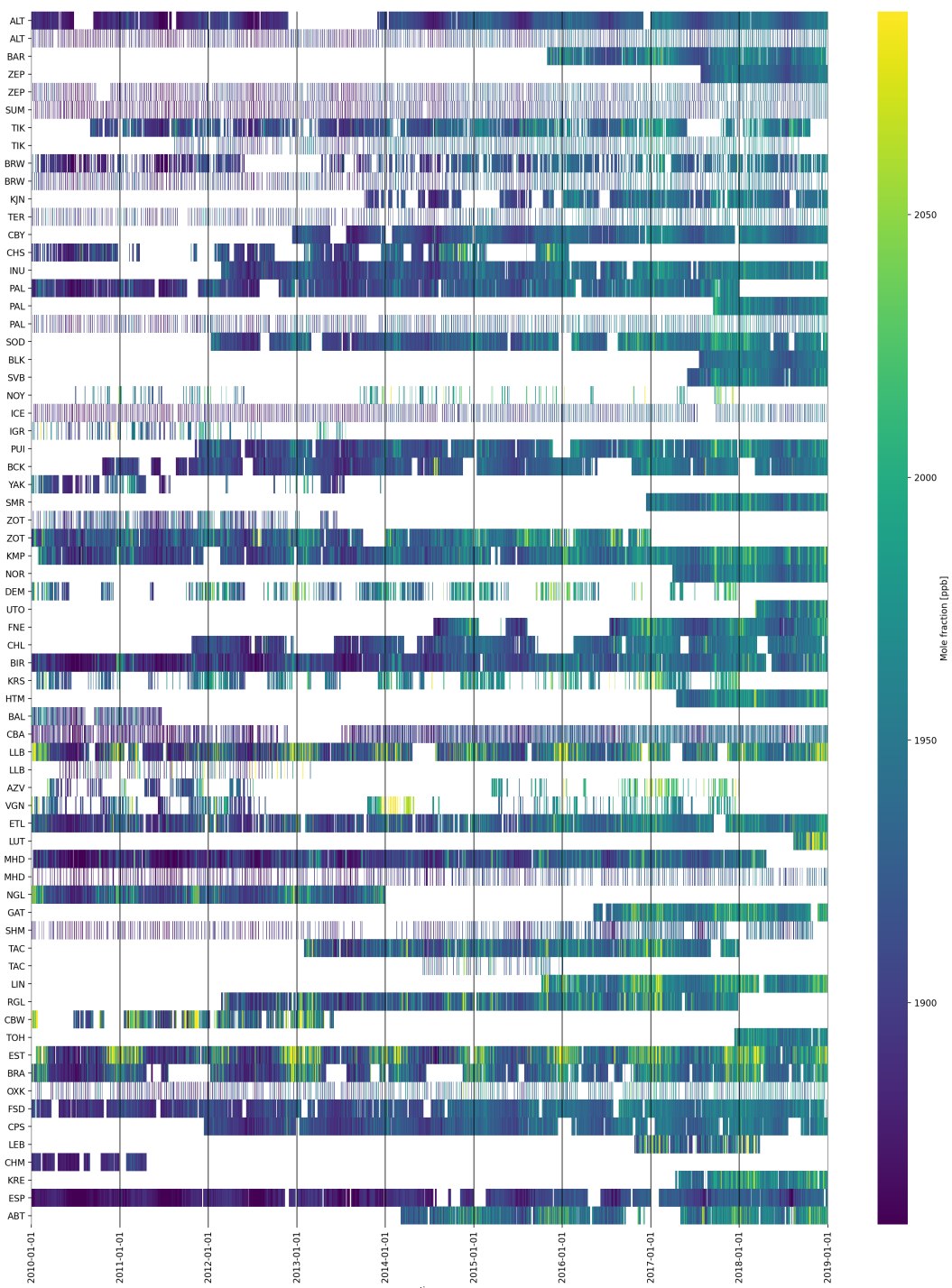


**Figure S1.** Daily averaged  $\text{CH}_4$  mole fraction observations [ppb] in measurement stations in years 2010–2018. Stations are ordered by their latitudes (the northernmost at the top and the southernmost at the bottom, only stations above 49°N are shown).

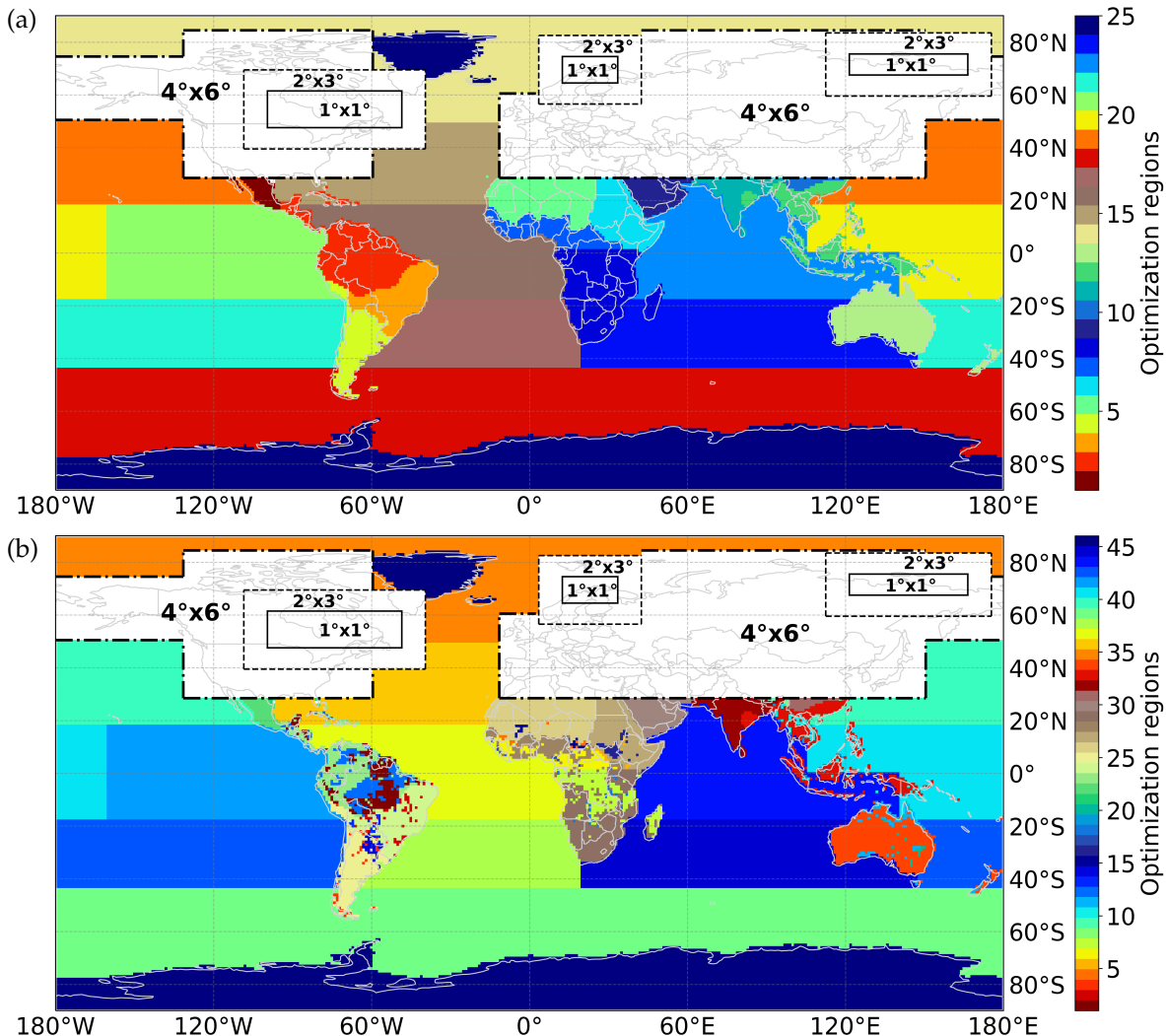


**Figure S2.** Figure illustrates the optimisation regions, a) anthropogenic and b) biospheric sources. We applied grid-based optimisation in the NH Temperate to Arctic regions, where observation network is the most dense. For other areas, region-wise optimisation is used, where the regions are defined based on modified TransCom regions and soil-type distribution from LPX-Bern DYPTOP model.

The grid-based optimisation is applied to the NH Temperate to Arctic regions.  $1^\circ \times 1^\circ$  latitude  $\times$  longitude grid-based optimisation is applied to the wetland regions (R1), surrounded by  $2^\circ \times 3^\circ$  intermediate grids (R2). Elsewhere we have  $4^\circ \times 6^\circ$  optimisation resolution (R3). We applied correlation lengths of 100, 200 and 500 km, for R1, R2 and R3, respectively. The correlation length for region-wise optimisation regions is 500 km over land and 900 km over ocean.

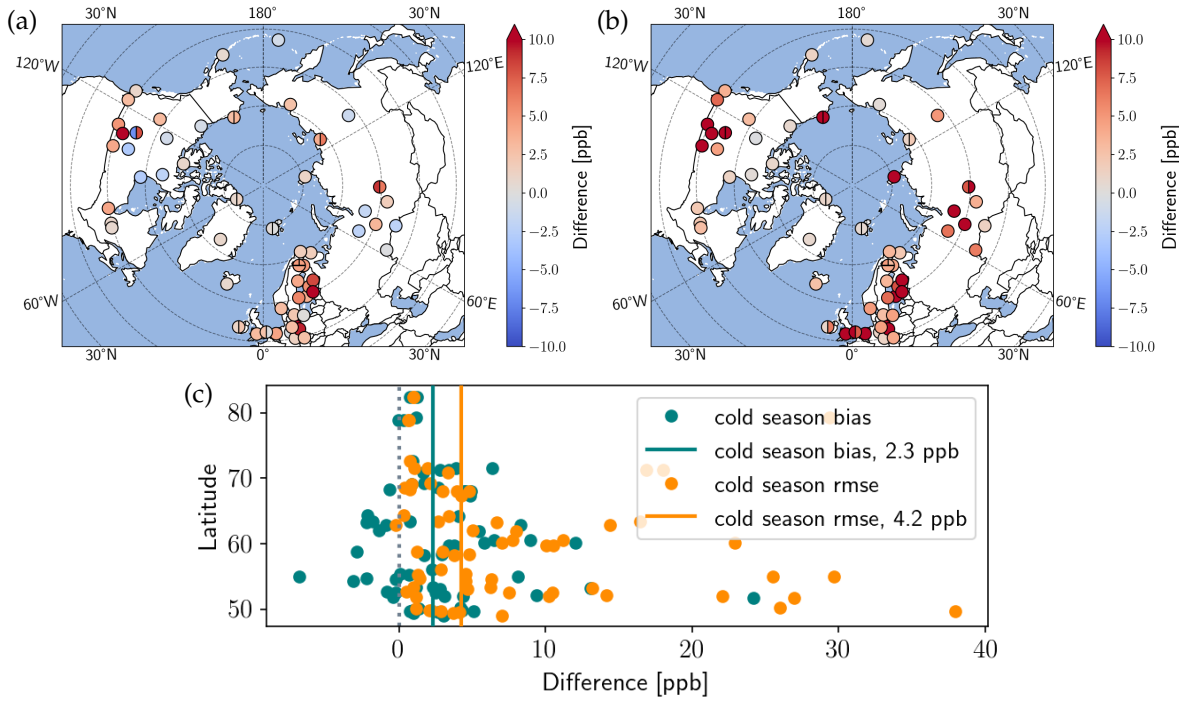


**Figure S3.** Differences in cold season biases (a) and in RMSEs (b) between mole fractions modelled with TM5 using LPX as a biospheric a priori and optimised mole fractions from CTE FT. The statistics are calculated against observations, i.e. model–observations. Positive values denote improvement in agreement with the observations, i.e. decreases in biases and RMSE, and negative values denote worsened agreement. c) The cold season bias and RMSE differences between mole fractions modelled with TM5 using LPX as a biospheric a priori and optimised mole fractions from CTE FT by latitudes. Median values are denoted with the solid vertical lines.

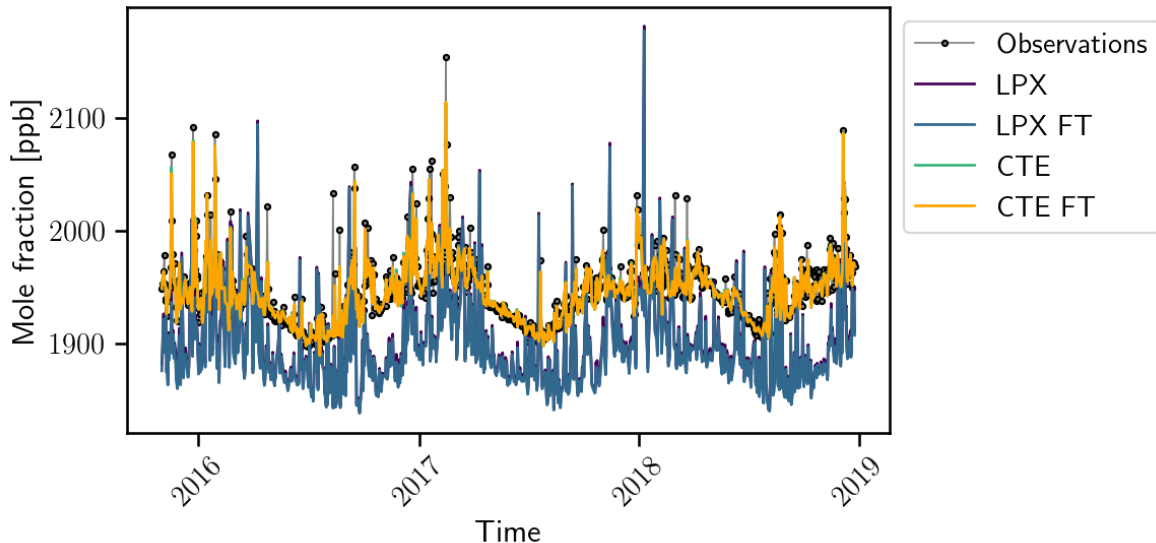


**Figure S4.** Observed and modelled CH<sub>4</sub> mole fractions at Baranova, Russia (79.28°N, 101.62°E). Modelled mole fractions without optimisation (LPX, LPX FT as the biospheric a priori) and with optimisation (CTE, CTE FT) are shown.

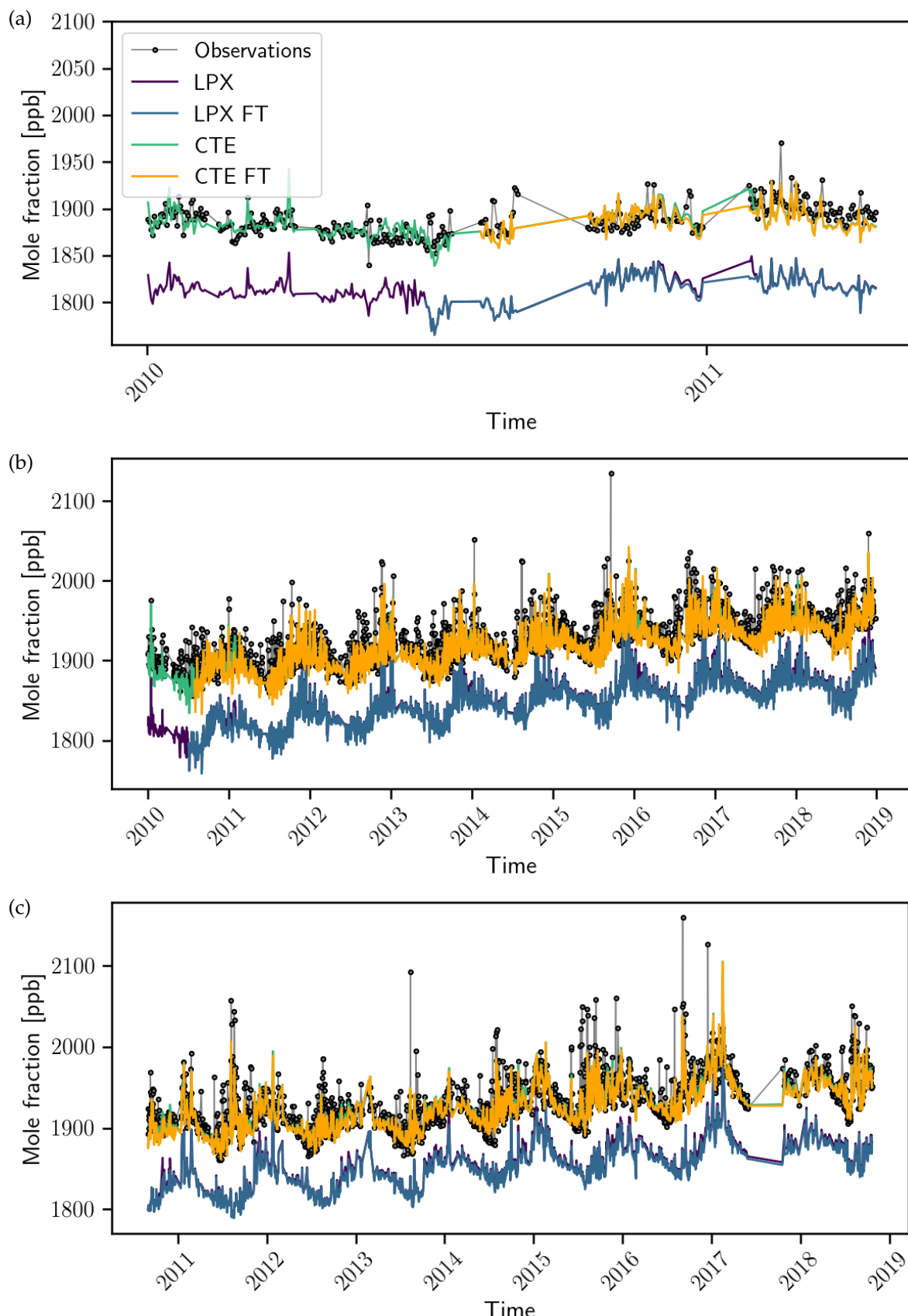


**Figure S5.** Observed and modelled  $\text{CH}_4$  mole fractions at selected measurement sites. Observations are daily averages used in the inversion (Section 2.3). Modelled mole fractions without optimisation (LPX, LPX FT as the biospheric a priori) and with optimisation (CTE, CTE FT) are shown. a) Chibougamau, Canada, ( $69.13^\circ\text{N}$ ,  $105.06^\circ\text{W}$ ). b) Fraserdale, Canada ( $49.88^\circ\text{N}$ ,  $81.57^\circ\text{W}$ ). c) Tiksi, Russia, ( $71.60^\circ\text{N}$ ,  $128.89^\circ\text{E}$ ).

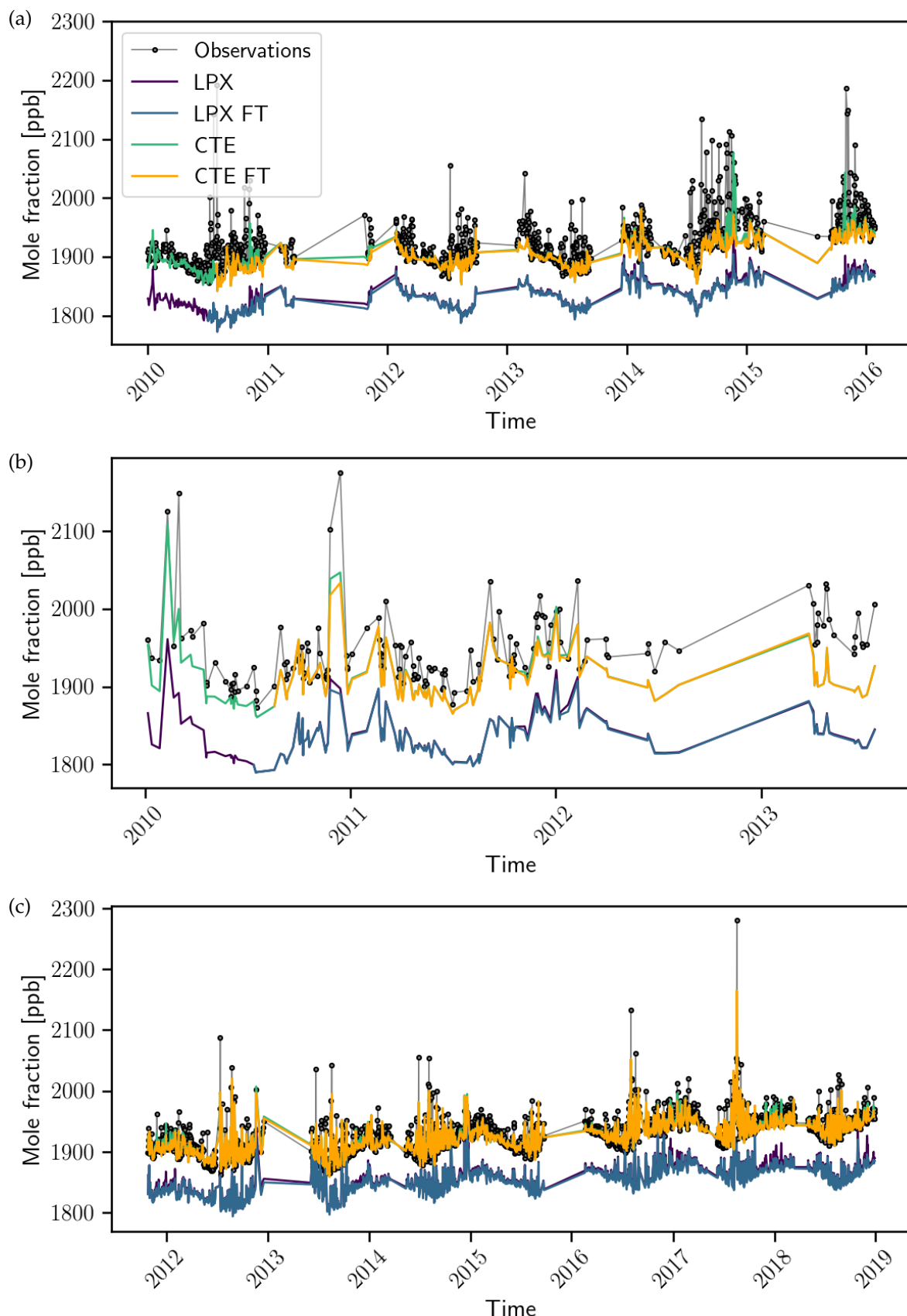


**Figure S6.** Observed and modelled  $\text{CH}_4$  mole fractions at selected measurement sites. Observations are daily averages used in the inversion (Section 2.3). Modelled mole fractions without optimisation (LPX, LPX FT as the biospheric a priori) and with optimisation (CTE, CTE FT) are shown. a) Cherskii, Russia ( $68.51^\circ\text{N}$ ,  $161.53^\circ\text{E}$ ). b) Igrim, Russia ( $63.19^\circ\text{N}$ ,  $64.41^\circ\text{E}$ ). c) Churchill, Canada ( $58.74^\circ\text{N}$ ,  $93.82^\circ\text{W}$ )

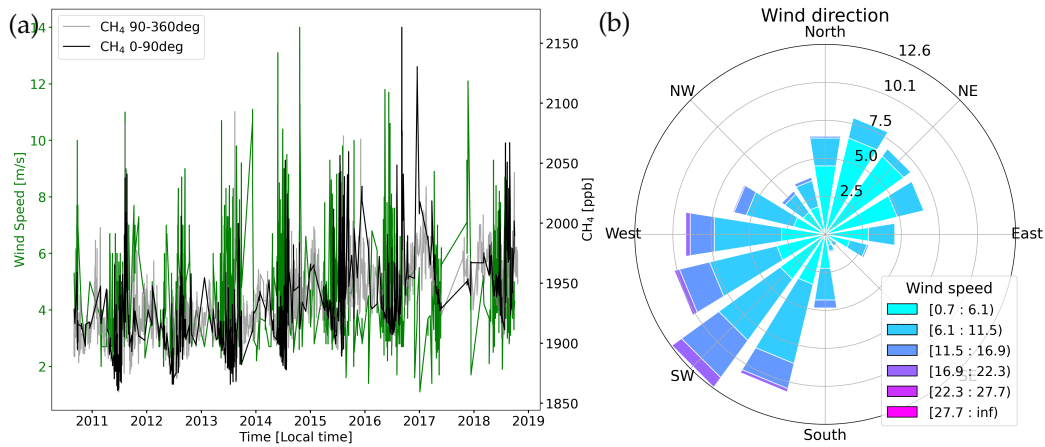


**Figure S7.** a) Wind speed and methane concentration at Tiksi site. The observations are hourly means from 12 pm to 16 pm and filtered based on a quality flag. Northeastern ( $0^\circ$ - $90^\circ$ ) wind, i.e., wind blowing from the direction of a nearby city, is highlighted with green. b) Wind speed and direction distribution at Tiksi site.

**Table S2.** Annual and cold season average biospheric methane emissions of EDGAR v5.0 and CTE FT, differences between CTE and CTE FT and the ratio of the difference to the CTE FT emissions. The uncertainties are one standard deviation of ensemble distributions. Global emissions and emissions in the northern high latitudes (NHL), in Western Siberian Lowlands (WSL) and Hudson Bay Lowlands (HBL) are shown.

Annual anthropogenic CH <sub>4</sub> emissions	Global	NHL	WSL	HBL
EDGARv5 [Tg/year]	$361 \pm 57$	$33.2 \pm 4.7$	$6.5 \pm 2.0$	$0.005 \pm 0.001$
CTE FT [Tg/year]	$375 \pm 54$	$36.3 \pm 3.8$	$7.3 \pm 1.9$	$0.005 \pm 0.001$
Diff CTE-CTE FT [Tg/year]	-0.69	-0.24	-0.10	$-6 \times 10^{-6}$
Ratio (diff/CTE FT) [%]	-0.18	-0.67	-1.4	-0.1
Cold season anthropogenic CH <sub>4</sub> emissions	NHL	WSL	HBL	
EDGARv5 [Tg/season]	$16.6 \pm 2.4$	$3.2 \pm 1.0$	$0.002 \pm 0.001$	
CTE FT [Tg/season]	$17.7 \pm 1.9$	$3.5 \pm 0.9$	$0.002 \pm 0.001$	
Diff CTE-CTE FT [Tg/season]	-0.23	-0.10	$-8 \times 10^{-6}$	
Ratio (diff/CTE FT) [%]	-1.3	-2.7	-0.3	